ELSEVIER

Physics of the Earth and Planetary Interiors 126 (2001) 93–108

PHYSICS OF THE EARTH AND PLANETARY INTERIORS

www.elsevier.com/locate/pepi

Rock-magnetic properties of TRM carrying baked and molten rocks straddling burnt coal seams

Cor B. de Boer*, Mark J. Dekkers, Ton A.M. van Hoof

Paleomagnetic Laboratory 'Fort Hoofddijk', Faculty of Earth Sciences, Utrecht University, Budapestlaan 17, 3584 CD Utrecht, The Netherlands

Received 30 November 2000; accepted 7 June 2001

Abstract

The subsurface spontaneous combustion of coal seams in Xinjiang (NW China) during Pleistocene to recent times produced large areas of thermally altered sedimentary rocks with large magnetic moments. The natural remanent magnetization (NRM) and thermoremanent magnetization (TRM) intensities and low-field susceptibilities of such combustion-metamorphic rocks range from 0.1 to 10 A/m and 100×10^{-4} to 1000×10^{-4} SI, respectively, which is two to three orders of magnitude higher than values typical of their sedimentary protoliths. The dominant magnetic carriers in the burnt rocks appear to include relatively pure forms of magnetite, maghemite and hematite as well as more complex spinel phases. These magnetic phases

(SD) inclusions in host silicate phases, which prevent them from oxidizing. The SD αFe particles can carry a highly stable remanence, having remanent coercivities ranging 70−140 mT. The ARM and IRM stability of all burnt rock samples to alternating fields is shown to be relatively high; median destructive fields, $B_{(1/2)A}$ and $B_{(1/2)I}$, respectively, range of 25−46 and ∼20−30 mT for dominant spinel-bearing samples, 34−36 and 47−53 mT for maghemite–hematite-bearing samples, and 48−89 and 64−84 mT for metallic iron-bearing samples. Consequently, burnt rocks are high-quality geomagnetic field recorders. Their very nature makes them useful for paleointensity determinations, although age determination is a limiting factor. Furthermore, remanence intensities and susceptibilities of these magnetically enhanced rocks are sufficient to produce observable magnetic anomalies. This property illustrates the potential to delineate the areal extent and depth of (extinct) coal fires with magnetic exploration. Such information is necessary to refine estimates of hazardous CO_2 emission and furthers our understanding of natural coal fires.

Keywords: Combustion-metamorphic rocks; Coal fires; Metallic iron; Rock-magnetism

1. Introduction

Baked and fused rocks produced by the subsurface spontaneous combustion of coal seams are common geologic features in many countries throughout the world, e.g. US (Foit et al., 1987; Cosca et al., 1989), India (Prakash et al., 1997), Romania (Rădan and Rădan, 1998), Czech Republic (Tyráček, 1994), Australia (Ellyett and Fleming, 1974), New Zealand (Lindqvist et al., 1985) and China (Zhang, 1998). In northern China, these so-called pyrometamorphic or combustion-metamorphic rocks are scattered over an enormous area stretching 5000 km EW and 750 km NS (Guan, 1984, 1989). In this region alone, already

* Corresponding author.
E-mail addresses: cor@stw.nl (C.B. de Boer), dekkers@geo.uu.nl (M.J. Dekkers).

0031-9201/01/$ – see front matter
PII: S0031-9201(01)00246-1

more than 100 active coal fire areas were detected in 55 coal fields, some of which have been burning for several hundreds of years (Guan, 1984; Kang et al., 1993; Van Genderen et al., 1996; Guan et al., 1996). The combustion-metamorphic rocks, however, are not restricted to active coal fires. In Xinjiang (NW China), for instance, Zhang (1998) and de Boer (1999) showed that spontaneous combustion of coal seams has occurred repeatedly during the recent geologic past; over 90% of the burnt rocks recognized in remote sensing imagery were associated with extinct coal fires and are mainly of Pleistocene age.

Combustion-metamorphism generally occurs at high (>600°C) to ultra-high (>1000°C) temperatures and low pressures (≤100 MPa). However, the degree of thermal alteration produced by burning coal beds is variable, and a single outcrop may contain altered rocks ranging from slightly baked to entirely fused (cf. Cosca et al., 1989). In close proximity to the burning coal seam and especially near vents and cracks in the overlying rocks (fresh oxygen supply) extreme temperatures up to 1500–2100°C can be reached (e.g. Bentor et al., 1981; Guan, personnel communication). Indeed, the (partially) fused and often highly vesicular rocks resemble blast furnace slags to a large extent, both in appearance and mineralogy.

The few paleomagnetic studies on these thermally affected rocks indicate that they can be high-fidelity geomagnetic field recorders (Jones et al., 1984; Krsová et al., 1989; Tyráček, 1994; Rădan and Rădan, 1998) possessing a well-defined and well-grouped thermoremanent magnetization (TRM) and/or thermochemical remanent magnetization (TCRM) that yield good-quality demagnetization diagrams. Because of the substantial heating, the rocks generally are magnetically enhanced, resulting in high remanence intensities resembling those of typical extrusive rocks. In addition, results by Jones et al. (1984) on baked rocks from Wyoming — although of preliminary nature — suggest that combustion-metamorphic rocks have potential to provide a high-resolution recording of the geomagnetic field, at least for much of the Quaternary, because the baked rocks show some level of secular variation. Because of a favorable coal-seam/topography relationship, the combustion-metamorphic rocks would represent a long duration. The fires started at the original outcrop with propagation rates that are nowadays reasonably well known (e.g. Kang et al., 1993). Therefore, the duration of a burning event can be assessed from how far burnt rocks are occurring from the original surface that usually can be estimated with sufficient certainty. Jones et al. (1984) argue that intermittent burning events (also in different coal seams) could be correlated by fission-track dating on zircons that also would provide absolute ages for (part of) the records, although the large errors inherent to the fission-track method are acknowledged. In the ideal situation, a more or less continuous composite record could be constructed. Although interesting from a paleomagnetic point of view, very little is known of the magnetic mineralogy that carries the TRM in these conspicuous rocks.

In this contribution, we report the rock-magnetic properties of burnt rock samples from outcrops exposed in the Toutunhe river area, located in the foothills of the Tian Shan Mountains, SW of Urumqi, the capital city of the Xinjiang Uygur Autonomous Region in NW China. The samples were obtained to better define their age using paleomagnetic methods. The characteristics of their natural remanent magnetization (NRM) and a brief description of the appearance of the burnt rocks at the sample sites are discussed in de Boer (1999) and Zhang et al. (in preparation). In this study area, spontaneous combustion of folded coal seams — varying in thickness from 1 to 27 m — has thermally altered overlying (and underlying) Jurassic deltaic siltstones, mudstones, and sandstones (Schneider, 1996), as well as Holocene river terraces. Typical thickness of the burnt rock deposits in the study area is 10−30 m, and the maximum thickness is ∼100−150 m.

2. Samples and equipment

Ten oriented hand samples were collected from four different age groups of burnt rocks spanning the Quaternary (Table 1). Because of their original paleomagnetic purpose, sampling was confined to areas where the burnt rocks were hard and coherent, least deformed, and showed evidence of high baking temperatures. Furthermore, the samples were largely confined to the bottom of the collapsed layer, to avoid reorientation after TRM acquisition. The NRM intensities, age estimates, and texture and color descriptions are summarized in Table 1. The oldest

Table 1
NRM intensities, ages estimates and some color and texture characteristics of the different burnt rock samples collected in the Toutunhe river area in NW China

Sample site	Code	Color	Texture	NRM (A/m)	Estimated age
Beigou	PMB1	Reddish-brown	Compact/breccious	0.189	Late Pliocene/early Pleistocene
	PMB2	Reddish-brown	Compact/breccious	0.178	Late Pliocene/early Pleistocene
Qianshuihe	PMQ1	Dark grey	Slightly vesicular	0.314	Middle Pleistocene
Louzhuangzi	PML3	Dark grey/black	Highly vesicular	0.741	Middle Pleistocene
Gangou	PMG1	Pale grey	Vesicular	0.002	Late Pleistocene
	PMG2	Pale grey	Vesicular	0.002	Late Pleistocene
Liugong	PML1	Pale grey	Slightly vesicular	0.879	Late Pleistocene
	PML2	Purple-black	Compact/fine-grained	5.789	Late Pleistocene
Kelazha	PMK1	Brownish-grey	Vesicular/breccious	1.824	Holocene/active fires
	PMK2	Tiger-striped	Relict structure/vesicular	0.779	Holocene/active fires

burnt rocks from the Beigou-group (PMB1 and PMB2) are compact reddish-brown materials that are slightly brecciated. The dark grey samples of middle Pleistocene age, PMQ1 and PML3, respectively, are slightly and highly vesicular with a 'sugary' appearance. PMQ1 weathers pale brownish. The late Pleistocene Gangou (PMG1 and PMG2) samples are (pale) grey vesicular with a variable brecciated character. Sample PMG1 has a brownish weathering color, whereas PMG2 has a pale yellowish-brown surface layer. The Liugong burnt rock samples (PML1 and PML2) belong to the same age group as Gangou: they are pale grey vesicular and black fine-grained compact rocks with a purple shade, respectively. PML1 has a brown-beige weathering color. The youngest burnt rocks that are associated with active coal fires, are labeled PMK1 and PMK2. PMK1 is a brownish-grey vesicular breccia with an orange-brown weathering color, and the slightly vesicular PMK2 sample is the only rock in which remnants of a relict bedding structure are still recognizable by a reddish tigerstripe pattern (millimeter scale). Apart from the Gangou samples, the NRM (TRM) intensities appear to be very high (0.2−5.8 A/m) when compared to NRM (post-depositional remanent magnetization, PDRM) intensities generally reported for their sedimentary protoliths (∼0.01−1 mA/m). Heating-induced mineral transformation magnetically enhanced these rocks. TRM acquisition without increased magnetic mineral content would also have led already to much higher NRMs because TRM is more efficient than PDRM. The combined effect has resulted NRM intensities in the burnt rocks that are several orders of magnitude higher than those typical of sedimentary protoliths.

The response of all burnt rock samples to alternating field (AF) demagnetization is excellent, the NRM demagnetization diagrams were of high quality. The determination of the characteristic remanent magnetization (ChRM) directions was straightforward, all samples reveal a univectorial decay to the origin (cf. de Boer, 1999; Zhang et al., in preparation). Only normal polarity ChRM directions were detected. Rock-magnetic investigations, undertaken to characterize the carriers of the remanence, included acquisition of anhysteretic remanent magnetization (ARM) and isothermal remanent magnetization (IRM), AF and thermal demagnetization, susceptibility measurements, and Curie temperature analysis. ARM and IRM measurements were performed on standard cylindrical samples that were sister specimens of those that were previously analyzed for their NRM behavior (cf. de Boer, 1999; Zhang et al., in preparation). Unfortunately, no sister specimen of sample PML2 was available or could be obtained from the hand sample by additional drilling. Before imparting ARM, the samples were AF demagnetized in a 0.3 T peak field to remove the high intensity NRMs. Anhysteretic remanences were progressively imparted using a laboratory-built AF demagnetizer coil with a maximum peak AF field of 0.3 T and a steady direct current (dc) biasing field of 16 μT which was parallel to the axis of the alternating field. The maximum ARM is labeled ARM (16 μT and 300 mT). An uniaxial (1 T) as well as a triaxial composite IRM (1 T, 120

and 20 mT), were acquired with a PM4 pulse magnetizer. The acquired remanences were measured on a digitized spinner magnetometer based on a Jelinek JR3 drive unit. Remanence intensities were at least an order of magnitude above the noise level in the instrument ($\sim$5 nA m^2). After acquisition was completed, the ARM and the single-axis IRM were stepwise AF demagnetized in peak fields up to 0.3 T, whereas the triaxial IRMs were progressively demagnetized by applying stepwise thermal demagnetization with 50 or 100°C temperature increments below 500 and with 20°C intervals up to 750°C. Thermal demagnetization was performed in a magnetically shielded laboratory-built furnace (residual field $<$ 20 nT). After each temperature step, the low-field bulk susceptibility was measured with a KLY-2 susceptibility bridge (AGICO, Brno; sensitivity 4×10^{-8} SI) by averaging measurements along three orthogonal sample axes. Thermomagnetic runs of crushed samples were recorded in air with an extremely sensitive, modified horizontal translation Curie balance making use of a cycling field (Mullender et al., 1993; sensivity of the balance is $\sim$5 nA m^2, allowing meaningful detection of weakly magnetic phases like hematite). Hysteresis loops and remanent coercivity curves were obtained at room temperature on rock chips of a few milligram using an alternating gradient magnetometer (Micro-Mag Model 2900, sensitivity $\sim$1 nA m^2, sample magnetizations were at least an order of magnitude higher).

3. Experimental results

The samples showed considerably varying mineral-magnetic behavior but can be broadly divided into three groups: (1) samples from Beigou; (2) samples from Quianshuihe, Liugong, Louzhuangzi, and Kelazha, all together referred to as QLLK group; and (3) samples from Gangou. For some hysteresis properties, and ARM and IRM intensities and properties, the grouping is not always that clear, therefore, results are presented method-wise. At the beginning of each subsection, the main sample grouping is given for the method followed by a discussion of the most prominent features per group. Thermal methods, in particular thermomagnetic analysis, get somewhat more emphasis because they yielded most meaningful information concerning the magnetic mineralogy, including the detection of metallic Fe.

3.1. Thermomagnetic analysis

The strong-field thermomagnetic behavior in air of the burnt rocks is usually characterized by more than one magnetic mineral (Fig. 1a–j). The Beigou samples contain hematite in addition to a maghemite-like spinel. The QLLK samples contain either a single magnetite-like spinel or multiple spinels including spinels with considerably lower Curie points (T_c). They do not contain hematite. The third group consists of the Gangou samples that contain metallic iron in addition to various spinels.

3.1.1. Beigou group

The heating curves of the reddish-brown Beigou samples (Fig. 1a and b) exhibit T_cs at $\sim$630 and 675°C, typical of nearly pure maghemite (γ-Fe_2O_3) and pure hematite (α-Fe_2O_3), respectively. The inflection at 410$-$420°C might represent the T_c of a spinel-type phase (substituted magnetite) or the irreversible transformation of the most fine-grained portion of the maghemite phase to less magnetic hematite. The latter option is favored as the cooling curve does not show the break in slope at 410$-$420°C. Most of the thermodynamically metastable maghemite, however, survives heating up to 700°C. Such 'high-temperature stability' is reported for relatively coarse-grained maghemite and slightly Al- and/or Ti-substituted maghemite varieties (e.g. Wilson, 1961; de Boer and Dekkers, 1996). Although both samples are magnetically dominated by highly magnetic maghemite, chemically they are fully dominated by hematite, because the spontaneous magnetization (σ_s) of γ-Fe_2O_3 is higher than that of α-Fe_2O_3 by two orders of magnitude. Estimated weight percentages of hematite and maghemite are 10$-$20% and $<$1%, respectively, based on their commonly reported σ_s values of 0.4 and 74 A m^2/kg. It is realized that hematite is not entirely saturated in the field available so that the percentage listed should be regarded as a minimum value.

3.1.2. QLLK group (Quianshuihe, Liugong, Louzhuangzi and Kelazha)

The Quianshuihe, Liugong, Louzhuangzi and Kelazha samples show variable thermomagnetic behavior.

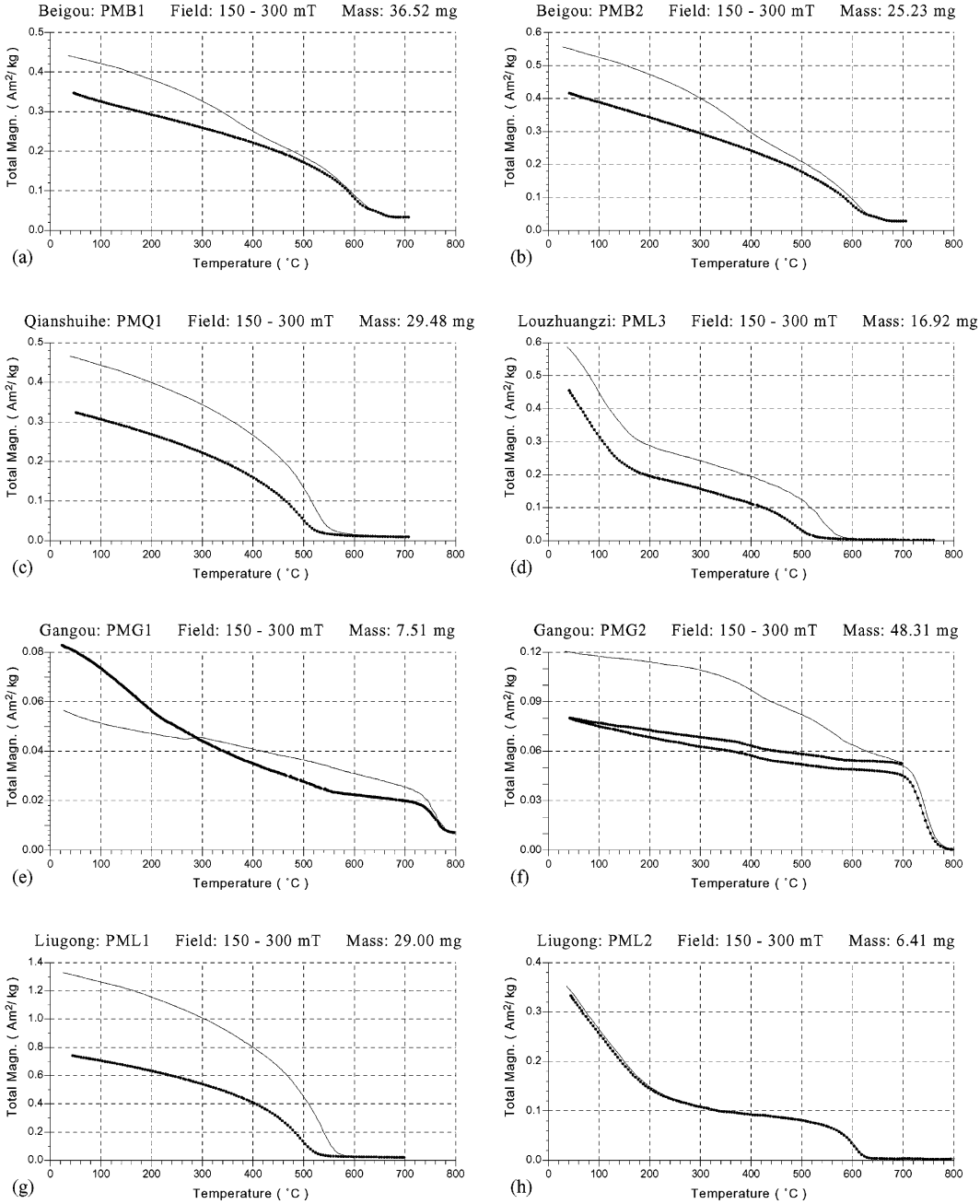

Fig. 1. Typical thermomagnetic curves measured in air of various combustion-metamorphic rocks. Thin solid lines and thick dotted lines denote heating and cooling runs, respectively.

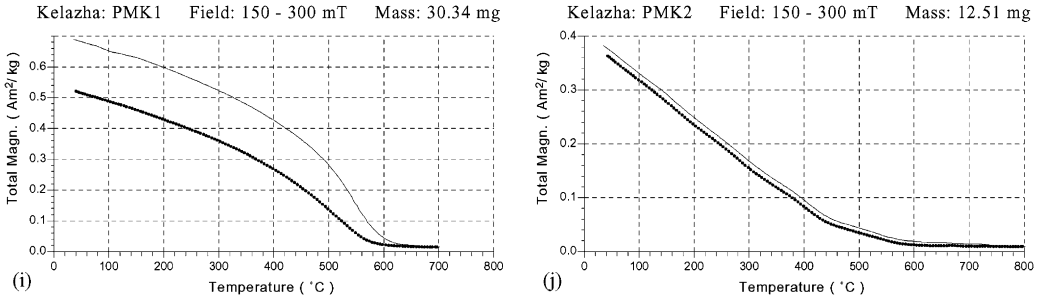

Fig. 1 (*Continued*).

Irreversible thermomagnetic curves with a single T_c at 550−600°C indicating compositions close to pure magnetite, characterize the samples PMQ1, PML1, and PMK1 from Quianshuihe, Liugong, and Kelazha, respectively (Fig. 1c, g and i). The small differences in Curie points are likely caused by slightly different degrees of isomorphous substitution and/or oxidation (cf. Dunlop and Özdemir, 1997). Weight percentages of the magnetic phase in these burnt rock types range between ∼0.5 and 1.5% (based on $\sigma_s = 92\,A\,m^2/kg$ at room temperature for pure magnetite). Samples PML3 from Louzhuangzi (Fig. 1d) and PML2 from Liugong (Fig. 1h) are both characterized by a low T_c (180−220°C) and a high T_c (570−620°C) magnetic mineral, likely representing members of the magnetite–maghemite series with a high and a low degree of isomorphous substitution, respectively.

3.1.3. Gangou group: traces of metallic iron

The Gangou group burnt rocks (Fig. 1e and f), which are significantly less magnetic (σ_s values: ∼0.06 and $0.12\,A\,m^2/kg$) than the other samples (σ_s values: ∼0.36–1.3 $A\,m^2/kg$), show the most conspicuous thermomagnetic behavior. The samples are characterized by traces of highly magnetic pure native iron (αFe; $T_c = 770$°C; Bozorth, 1961) which remarkably (partly) survives thermal cycling in air up to 800°C. This latter observation suggests that the αFe particles are present as tiny inclusions trapped in host minerals or that they are coated with a surface layer impermeable to oxygen, which prevent them from being oxidized. The detection of αFe in the burnt rocks is noteworthy because native iron is very rare in terrestrial rocks. Pure αFe has been described from only a few localities (e.g. Verma and Prasad, 1975; Deutsch et al., 1977; Haggerty and Toft, 1985) of which the most famous is Disko Island on West Greenland where huge iron boulders were formed after the incorporation of carbon-rich sediments into basalts during the extrusion (cf. Ulff-Møller, 1990).

The strong-field thermomagnetic behavior of sample PMG1 seems to be dominated by αFe, because no other Curie points are observed on the heating curve. The remarkable small break in slope at ∼270°C is reproducible in other subsamples; its cause, however, is not known. The estimated weight percentage of αFe in this sample, based on the initial magnetization of $\sim 0.057\,A\,m^2/kg$ and a σ_s of $217.75\,A\,m^2/kg$ (Bozorth, 1961), is only 0.026%. Sample PMG2 contains a comparable amount of αFe and additional traces of magnetite and a magnetic spinel phase with a T_c of ∼440°C. Sample PMK2 of the QLLK group (Fig. 1j) seems to contain the same magnetic mineralogy as sample PMG2, but is strongly dominated by the spinel phase with the T_c of ∼440°C. The Curie point of metallic iron is, therefore, hardly visible.

3.2. Hysteresis parameters

Basically three types of hysteresis loops were obtained: (1) distinctly wasp-waisted loops for the maghemite–hematite-bearing Beigou samples (Fig. 2a); (2) ramp-like loops for the αFe-bearing Gangou samples (Fig. 2b); and (3) 'regular' loops for the spinel-dominated samples, i.e. those from the QLLK group (Fig. 2c). Different spinels, however, do not show up by distinctly different hysteresis loops.

Wasp-waisted hysteresis loops are produced by a mixture of magnetically soft (maghemite) and hard (hematite) minerals only when the two phases

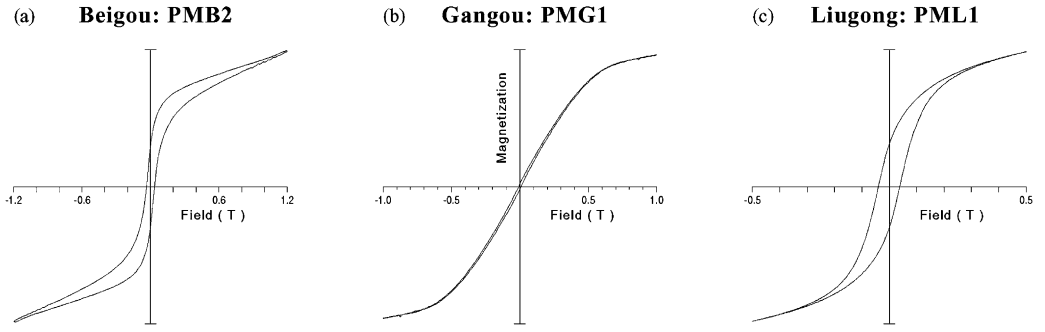

Fig. 2. Room temperature hysteresis loops typical of (a) maghemite–hematite-bearing samples; (b) native iron-bearing samples; and (c) spinel-bearing samples of combustion-metamorphic rocks. Magnetization (*y*-axis) is in arbitrary units.

contribute comparable amounts of magnetization (e.g. Roberts et al., 1995). As concluded before, this observation implies that hematite must be about 100 times as abundant in these rocks as maghemite to rival the latter contribution to magnetization. The coercive force (B_c) of ~30 mT and the remanent coercive force (B_{cr}) of ~100 mT — dominated by the maghemite and the hematite phase, respectively — point to stable single-domain (SD) to pseudo-single-domain (PSD) particles for both minerals (Table 2).

Ramp-like hysteresis curves are typical of either large multi-domain (MD) particles or of a mixture of super paramagnetic (SP) and SD particles. The relatively high B_{cr} values of 71 and 141 mT (Table 2) support the second option. The high B_{cr} values imply that the SD part of the αFe particles is able to carry a geologically stable remanent magnetization.

Thermomagnetic analysis indicated that samples PMQ1, PML1 and PMK1 (all QLLK group) contain a very dominant magnetic phase of near-magnetite composition and thus their hysteresis parameters can be interpreted in terms of magnetic grain size. The remanence (M_{rs}/M_s) and coercivity (B_{cr}/B_c) ratios for the three samples are characteristic of PSD grains implying that they can carry a stable NRM. The absence of meaningful viscosity makes the alternative possibility of superposed SD and SP grains (cf. Tauxe et al., 1996) highly unlikely. Although the hysteresis parameters obtained for the other samples cannot directly be interpreted in terms of magnetic grain

Table 2
Basic rock-magnetic parameters at room temperature for various burnt rocks[a]

Code	χ_{lf} (10^{-4} SI)	ARM (A/m)	$B_{(1/2)A}$ (mT)	IRM (A/m)	$B_{(1/2)I}$ (mT)	B'_{cr} (mT)	B_c (mT)	B_{cr} (mT)	B_{cr}/B_c	M_{rs}/M_s
PMB1	120	1.256	36	478	53	95	27.9	113.0	4.1	0.38
PMB2	111	1.120	34	406	47	77	33.1	86.8	2.6	0.51
PMQ1	151	0.497	25	492	23	58	14.2	44.5	3.1	0.14
PML3	329	1.198	33	>1000	20[b]	43[c]	29.9	57.5	1.9	0.32
PMG1	6.5	0.013	89	3	84	143	8.2	141.0	17.2	0.03
PMG2	6.5	0.008	48	8	64	144	4.7	71.2	15.2	0.08
PML1	113	0.815	45	616	30	64	39.1	64.0	1.6	0.42
PML2	955	nd	nd	nd	nd	nd	11.2	16.4	1.5	0.42
PMK1	604	2.948	46	>1000	28[b]	33[c]	26.1	65.1	2.5	0.36
PMK2	35	0.686	45	86	30	51	9.4	36.4	3.9	0.23

[a] Meanings of the parameters are explained in the text. Susceptibility and the ARM and IRM parameters were measured on standard 2.5 cm cylindrical samples, whereas the latter four hysteresis parameters were measured on small rock chips of a few milligrams using an alternating-gradient force magnetometer; nd: not determined.

[b] $B_{(1/2)I}$ is too high, because the IRM intensity of these samples lies beyond the measurable range after applying ~100 mT dc fields.

[c] B'_{cr} is too low, because the IRM intensity of these samples lies beyond the measurable range after applying ~100 mT dc fields.

size because their hysteresis loops are superimposed curves of different magnetically soft minerals, they probably also fall in the stable PSD range.

3.3. Acquisition and AF stability of ARM and uniaxial IRM

Apart from the relative low-intensity (∼10 mA/m) αFe-bearing Gangou samples, the ARM (16 μT and 300 mT) intensities of the burnt rocks show a narrow range of ∼0.5−2.9 A/m (Table 2, Fig. 3a–c). IRM (1 T) intensities behave in a similar way: they are ∼5 A/m for the comparatively weakly magnetic Gangou samples and range between 86 and ∼1200 A/m for the other samples (Table 2, Fig. 3d–f). Samples PML3 and PMK1 have intensities above the highest measurable intensity of 1000 A/m; extrapolation of their acquisition curves to 1 T yields values near ∼1200 A/m.

3.3.1. ARM properties

ARM (16 μT and 300 mT) intensities are of similar magnitude as the initial NRM intensities (cf. Table 1) measured on sister specimens. The fine-grained nature of the rocks as well as their mode of formation makes large differences in magnetic mineralogy unlikely on a centimeter scale. Therefore, we may compare sister specimens from the same drill cores. The ARM (16 μT and 300 mT)/NRM (intensity) ratio ranges 0.9–6.6; the higher values (4−6.6) are obtained on samples that contain a mixture of magnetically soft and hard minerals (i.e. the maghemite–hematite-bearing Beigou samples and the αFe-bearing Gangou samples), whereas the lower values (0.9−1.6) belong to samples that only contain relatively low-coercivity spinels. This observation shows that, compared to the NRM, the ARM favours the contribution of the soft minerals to the signal, hinting at possibly different grain-size trends for TRM and ARM (cf. Dunlop and Xu, 1993).

ARM acquisition shows that the burnt rock samples appear hard to saturate in the maximum available alternating field (Fig. 3b and c). PMQ1 (QLLK group) is the only sample that fully saturates in a 300 mT AF, while the other samples still show a more or less gradual increase in ARM values, implying the presence of magnetically relatively hard components. At 100 mT, the alternating field commonly used to induce an ARM, the ARM reaches ∼45 to 90% of the intensity obtained with 300 mT alternating fields. For sample PMG1 (Gangou), the presence of two magnetic phases with contrasting coercivities can clearly be deduced from the shape of the ARM acquisition and AF demagnetization curves. Based on their thermomagnetic curves and hysteresis parameters, the high-coercivity mineral likely is SD αFe, whereas the low-coercivity component that almost saturates and demagnetizes in AF fields of ∼20 mT might represent large MD or very small SD particles of αFe and/or spinel.

The resistance of the ARM against AF demagnetization is relatively high for all burnt rock samples. The ARM median destructive fields ($B_{(1/2)A}$) range of 25−89 mT. For the spinel-bearing samples (Fig. 3b) these values may be interpreted in terms of grain size and point to stable PSD particles. Their slightly S-shaped demagnetization curves support this suggestion; true SD grains show strongly sigmoid curves, while true MD grains show a more exponential decrease (e.g. Argyle et al., 1994). The ARM of sample PMQ1 (QLLK group) is carried by relatively large spinel particles which lie close to the MD side of the PSD range, while the particles of the other spinel-bearing samples lie closer to the SD side. The ARM of these samples (Fig. 3b) becomes fully demagnetized in 200 mT AF; samples shown in Fig. 3c require fields up to 300 mT. The ARM of sample PMK2 (QLLK group) could not be fully demagnetized in the maximum available AF. The cross-over ratio R between the ARM acquisition and demagnetization curves lies close to 0.5 for all samples. This observation implies that the ARM (16 μT and 300 mT) caring particles do not magnetically interact (Cisowski, 1981).

3.3.2. IRM properties

The normalized IRM acquisition curves show that the IRM of samples PMQ1 and PML1 (Fig. 3e) (both belonging to the QLLK group) is close to saturation (>97%) in 300 mT fields and fully saturates after applying 500 mT fields. B'_{cr} values are 58 and 64, respectively, implying PSD-type remanence carriers. Spinel-bearing samples PML3 and PMK1 (both QLLK group) likely exhibit similar behavior. On the other hand, the magnetically harder samples (Fig. 3f) not even fully saturate in 1 T dc fields. Their B'_{cr} values range of 51–144 mT. In general, the B'_{cr} and B_{cr} values of all samples match each other well, implying that the small rock chips on which the hysteresis

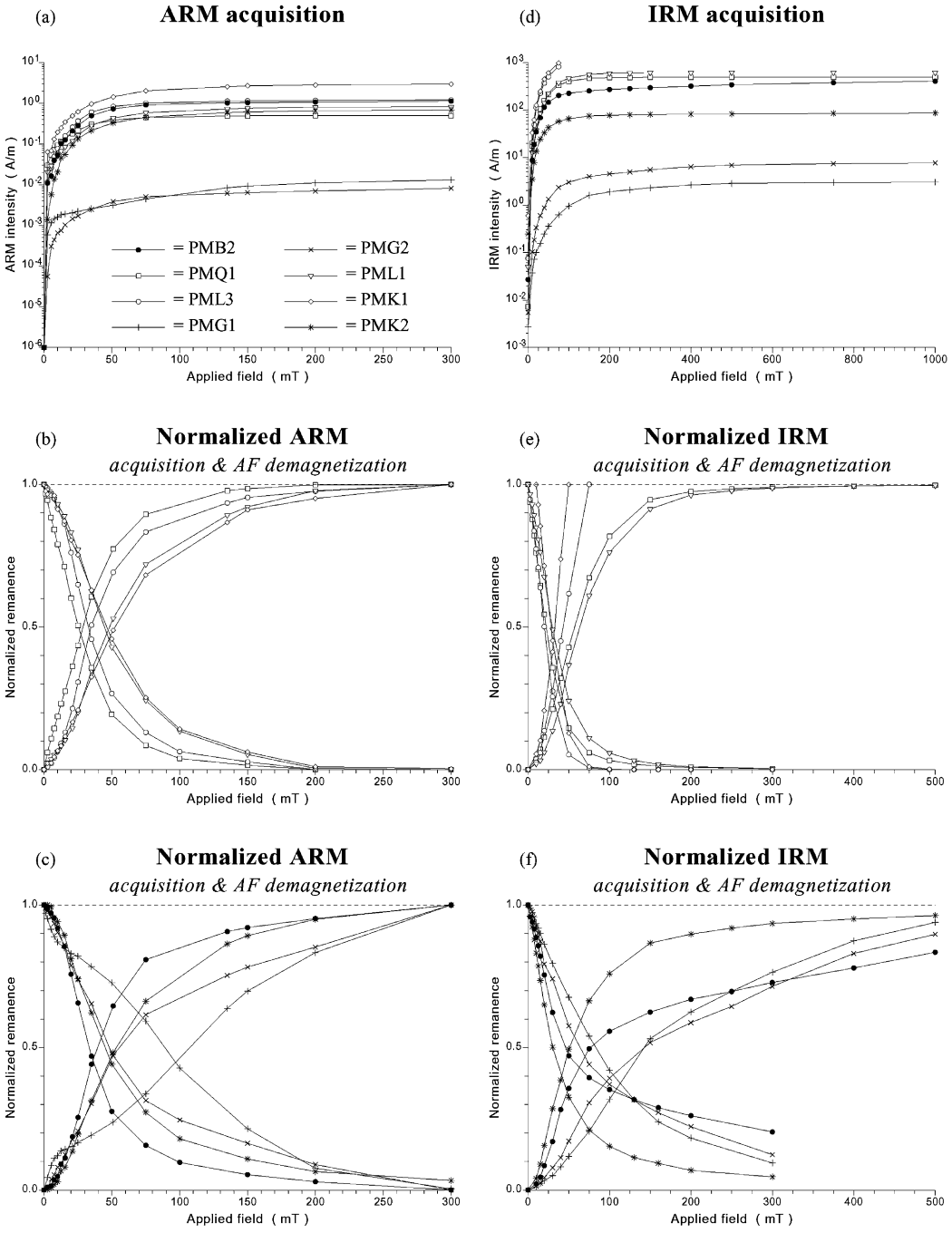

Fig. 3. (a–f) Typical acquisition and AF demagnetization curves of ARM and IRM for burnt rocks. Sample PMB1 and PMB2 show identical behavior. Therefore, only the results of sample PMB2 are plotted. The ARM dc bias field was 16 μT. IRM acquisition and AF demagnetization curves of panels (e and f) are normalized to the intensity acquired at 1 T. The IRM intensity of samples PML3 and PMK1 exceeds the highest measurable intensity in dc fields smaller than 100 mT.

parameters were determined contain magnetic minerals similar in grain size and type as those present in the larger cylindrical samples.

Samples with the highest final IRM (1 T) intensities, PML3 and PMK1 (both QLLK group), are least resistant to alternating fields and are already fully demagnetized in fields of 50−75 mT. Note that their IRM (1 T) intensities lie beyond the measuring range of the magnetometer; their demagnetization curves are normalized to the first measurable values after applying alternating fields during demagnetization. The other spinel-bearing samples (Fig. 3e) have values for the median destructive field of the IRM ($B_{(1/2)I}$) of 23 and 30 mT, but are only fully demagnetized after applying 0.3 T AF. The ratio $B_{(1/2)A}/B_{(1/2)I}$ exceeds one for these two samples, which supports their suggested PSD size, according to the ARM version of the Lowrie–Fuller test (Lowrie and Fuller, 1971). Samples shown in Fig. 3f again exhibit a much higher AF stability than the aforementioned spinel-bearing samples. Their $B_{(1/2)I}$ values range of 30–84 mT, and the IRM induced in 1 T dc fields of neither sample becomes fully demagnetized after applying ac fields up to 0.3 T.

The cross-over ratio *R* between the IRM acquisition and demagnetization curves ranges ∼0.3−0.4 which is considerably lower than for the ARM experiment. The acquisition of weak-field ARM and strong-field IRM and their respective AF demagnetization are dominated by slightly different factors. This is an indication that the internal demagnetizing fields of the remanence carrying minerals are more important in IRM than in ARM experiments (cf. Argyle and Dunlop, 1990). The low value of the ARM would correspond to a lower internal demagnetizing field than the high value of the IRM. Small grains are also more susceptible to ARM than IRM (cf. Jackson, 1991). The IRM (1 T)/ARM (16 μT and 300 mT) ratio is highly variable, ranging ∼125–1000, likely implying that the two remanent magnetizations are dominated by different coercivity fractions.

3.4. Susceptibility behavior and thermal stability of composite IRMs

3.4.1. Susceptibility behavior

Thermal demagnetization of the three orthogonal components of the composite IRMs (Fig. 4a–g) yields information on the remanence-carrying phases and their relative quantities to the signal, complementing the information gathered from thermomagnetic experiments. Heating, however, can induce alterations in magnetic mineralogy which may interfere with the demagnetization process. For this reason, the low-field susceptibility was measured at room temperature after each heating step (Fig. 4h). The unheated samples exhibit high initial χ_{lf} values, varying between 6×10^{-4} and 604×10^{-4} SI; variation in three orthogonal directions was insignificant for all samples.

For the QLLK group samples, no major changes in χ_{lf} were observed during the entire demagnetization treatment up to 750°C. This indicates that their magnetic mineralogy was stabilized, chemically and physically, at high temperatures. The χ_{lf} of αFe-bearing Gangou and maghemite–hematite-bearing Beigou samples hardly changes up to 600°C. Heating the samples above this temperature, however, results in a χ_{lf} increase, which continues up to the final heating step of 750°C. This χ_{lf} increase does not necessarily imply the creation of a new magnetic mineral, it may also be caused by a reduction in grain size of the existing minerals transforming PSD and/or SD particles to highly magnetic, yet unstable SP particles.

3.4.2. Thermal stability of composite IRMs

For the Beigou samples (Fig. 4a and b) the intermediate- and high-coercivity components contribute equally to the initial IRM. A magnetic phase with an unblocking temperature of ∼630°C contributes to all three coercivity fractions, but mainly dominates the intermediate component. This phase likely is near-pure maghemite of dominantly PSD size. The high-coercivity component is dominated by 680°C unblocking temperature, implying the presence of PSD to SD hematite.

QLLK group samples (PMQ1, PML1, and PMK2 respectively, Fig. 4c, d and g) are characterized by only one remanence carrying phase, of mainly intermediate coercivity, and with a maximum unblocking temperature of ∼580−600°C indicating the presence of a spinel-phase of near-magnetite composition. The contribution of the high-coercivity fraction to the signal is equal to or higher than the low-coercivity fraction suggesting that most particles lie on the near-SD side of the PSD range.

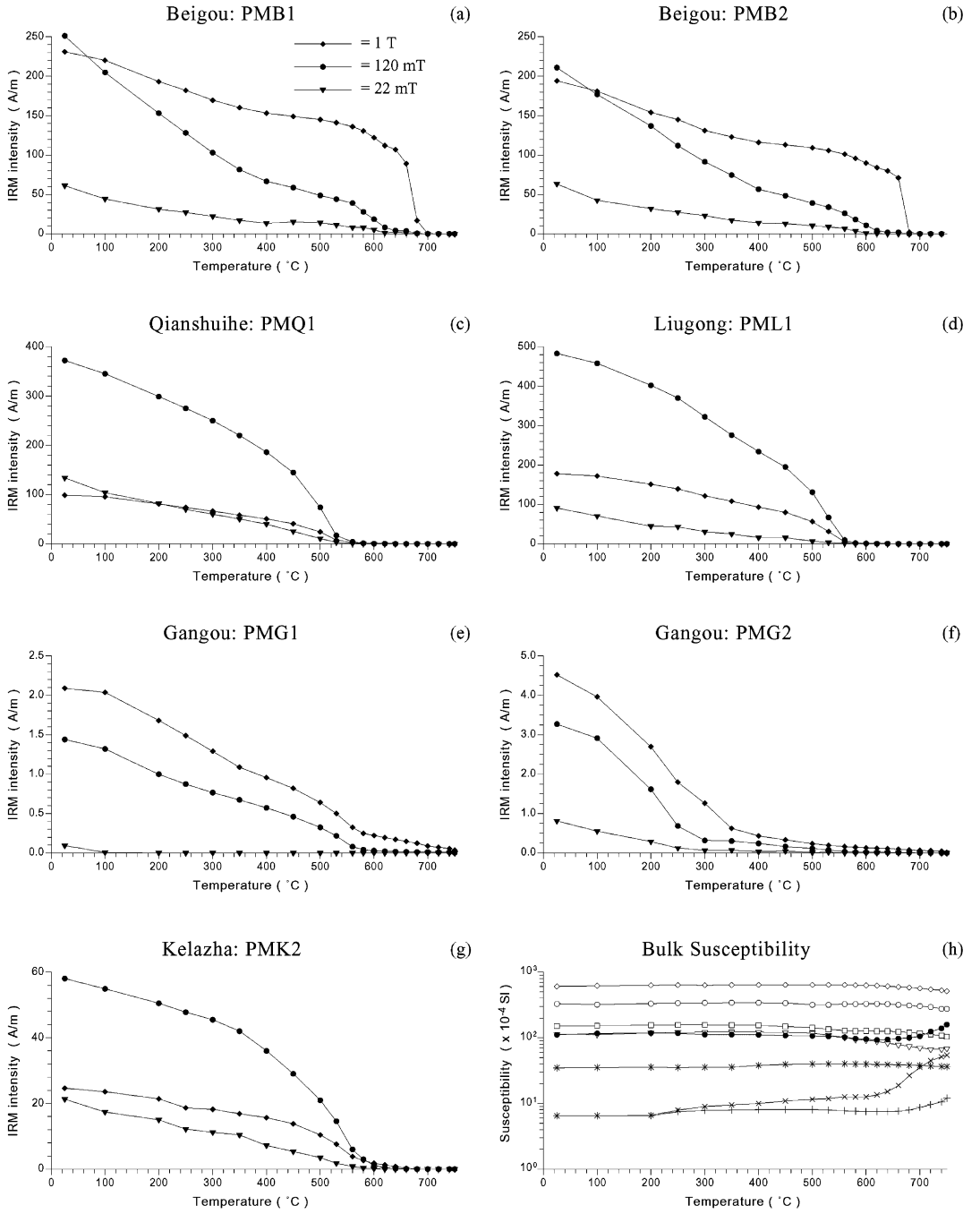

Fig. 4. (a–g) Stepwise thermal demagnetization of composite IRMs (cf. Lowrie, 1990) showing the different remanence carrying minerals in combustion-metamorphic rock samples. The high- (1 T), intermediate- (120 mT), and low-coercivity (22 mT) fractions are denoted with diamonds, circles, and triangles, respectively. (h) Bulk susceptibility measured at room temperature after each temperature step. Symbols as in Fig. 3.

The IRM of the Gangou-samples (Fig. 4e and f) is dominated by high- and intermediate-coercivity minerals. The intermediate-coercivity component unblocks at ∼580 and 300°C for sample PMG1 and PMG2, respectively. The lower unblocking temperatures indicate the presence of a spinel phase with considerable isomorphous substitution or the dominance of small particles. Identical spinel phases also dominate the high-coercivity component of both samples. A considerable fraction of the remanence, however, is only completely unblocked after heating at temperatures up to 750°C, indicating the presence of αFe. The high remanent coercivities of the spinel phases, and especially that of αFe, suggests that these phases are present as more or less elongated SD particles.

4. Discussion: implications and applications

4.1. Magnetic minerals and their appearance

The intense heat generated by spontaneous subsurface combustion of coal seams completely metamorphosed the overlying sediments to multi-colored burnt rocks varying in appearance from dense to vesicular or scoriaceous. The substantial susceptibility enhancement of these thermally-altered rocks compared to their sedimentary protoliths, indicates that new magnetic minerals were created during metamorphism. Indeed, the formation of abundant magnetic accessory phases is a phenomenon commonly associated with thermal alteration of many non-magnetic Fe-bearing minerals. Thermomagnetic analyses and stepwise thermal demagnetization of composite IRMs showed that burnt rocks produced from mudstones, siltstones and sandstones may contain a wide range of magnetic minerals including pure forms of metallic iron, magnetite, maghemite and hematite as well as impure magnetite phases with differing amounts and/or types of isomorphous substitution and/or different oxidation degree. The paleomagnetic samples may contain only one single magnetic mineral, but often show multiple magnetic phases.

The magnetic mineral assemblage encountered in burnt rocks depends on many physical and chemical parameters, including the original sediment bulk composition, temperature, degree of melting, and oxidation state (cf. Cosca et al., 1989). The extreme differences in oxidation degree between the magnetic mineralogy of the maghemite–hematite-bearing Beigou samples and the αFe-bearing Gangou samples indicate that the conditions during combustion may range from oxidizing to very reducing. In this context, the supply of fresh air to the rocks and their permeability are important factors. Oxidizing conditions may prevail during initial ignition of the coal layer at the outcrop or in the vicinity of cracks and vents in the overlying rocks after the coal fire propagated itself subsurface. Gleason and Kyser (1984) recognized that groundwater may be involved as an oxidant as well. The high amount of hematite (10−20 wt.%) in the Beigou burnt rocks may indicate that they are produced from ‘red bed’-like sediments already rich in α-Fe_2O_3 and/or goethite (α-FeOOH). The αFe-bearing burnt rocks are the least magnetic samples. Their protoliths likely are mature well-cemented sandstones relatively low in Fe-bearing minerals and highly impermeable to oxygen. Additional oxidation of minor incorporated organic matter during heating may have caused the extremely low oxygen fugacity required.

The Fe-bearing precursor minerals of the magnetic phases, based on their sedimentary protoliths, likely are clay minerals, ferromagnesian silicates and/or pyrites. Consequently, the most abundant ‘foreign’ cations substituting for Fe in magnetic iron oxides will be Al, Mg and Ti. Indeed, in petrographic studies on glass-bearing burnt rocks from Wyoming, Foit et al. (1987) and Cosca et al. (1989) recognized members of the magnetite–hercynite ($FeAl_2O_4$), ulvöspinel (Fe_2TiO_4) solid-solution series, the hematite–ilmenite ($FeTiO_3$) solid-solutions series, and solid-solution series from magnesioferrite along the spinel ($MgAl_2O_4$)–magnesioferrite ($MgFe_2O_4$) join to $Sp_{80}Mf_{20}$ and along the magnesioferrite–hematite join to $Mf_{60}Hm_{40}$. Most compositions of the latter two solid solution series lie in the Al-rich field and have formulas that are slightly cation deficient. Typical high temperature non-magnetic minerals encountered in combustion-metamorphic rocks appear to include several Fe and Al-rich clinopyroxenes, melilite solid solutions, crystobalite, tridymite, mullite, cordierite and fayalitic olivine as well as minor glass (e.g. Foit et al., 1987; Cosca et al., 1989; Rădan et al., 1994).

The rock-magnetic properties of the samples inspected indicate that most magnetic iron oxide

particles grew to PSD size during metamorphism. Native iron, on the other hand, occurs as tiny SP and SD particles. For equidimensional αFe-particles, the lower and upper limits for SD behavior are ∼0.008 and 0.023 μm, respectively (Kneller and Luborsky, 1963). Based on their high remanent coercivities, SD native iron, however, more likely is present as (slightly) elongated grains of which the SD range is broader compared to equant grains. The αFe-particles survive heating in air, and we envisage that they occur as inclusions encased in host minerals largely impermeable to oxygen. Furthermore, the cross-over ratio R appeared to be <0.5 for IRM carrying minerals which might indicate some degree of magnetic interaction between these particles. Consequently, a part of individual magnetic grains may occur as closely spaced aggregates or magnetic interaction exists between different parts of inhomogenous grains.

The characteristics of the magnetic minerals deduced from their rock-magnetic properties is consistent with the few available descriptions of iron oxides observed in thin sections of burnt rocks. Foit et al. (1987) and Cosca et al. (1989) reported that the iron oxides range in size from tiny euhedral crystals to large irregular masses and stringers hundreds of micrometers long. Most iron oxide masses and euhedra have been unmixed upon cooling to produce more or less complex two-phase intergrowths. Consequently, relatively pure magnetite or hematite phases are present as numerous geometrically arranged blebs or lamellae (sometimes in typical boxwork patterns) encased in iron oxide host minerals with substantial isomorphous substitution. The host oxides are the magnetic phases with relatively low Curie points.

4.2. Disorder and irreversible thermomagnetic behavior

Noteworthy is the 30−50°C shift of the Curie points to lower temperatures of some samples from the spinel-bearing QLLK group on cooling from 700°C (PMQ1, PML1, PML3, and PMK1; see Fig. 1c, d, g and i). This shift cannot be explained by experimental error, because temperature lag (1°C) is insignificant (see the behavior displayed in Fig. 1a, b and h). This typical behavior, however, could be caused by a heating-induced change of cation ordering. The Curie temperature of spinel-phases can be very sensitive to the intracrystalline distribution of Fe and 'foreign' cations between tetrahedral and octahedral sites of the spinel crystal structure. Harrison and Putnis (1999) showed that T_c appears to decrease with increasing disordering. For near-stoichiometric magnesioferrite ($MgFe_2O_4$), the authors obtained differences up to 60°C between the equilibrium ordered phase ($T_c = 364$°C) and more disordered phases. In our case, this could imply that heating induced some degree of disordering of the cations which remains on cooling, resulting in the observed decrease in T_c. In this view, the decrease in magnetization observed on cycling might be explained by a lower spontanous magnetization of the disordered phase compared to the initial ordered phase, rather than by heating-induced oxidation. The latter process also reduces the magnetization but generally increases the Curie temperature.

4.3. Application of the magnetic properties of combustion-metamorphic rocks

4.3.1. Geomagnetic field recording

The magnetic properties of the combustion-metamorphic rocks, especially those in the vicinity to the remaining ash layer of the coal seam, implies that they, in principle, are high-fidelity geomagnetic field recorders. Therefore, reliable determinations of absolute paleointensities and of magnetic reversals records should be possible. The rocks are strongly magnetized and the minerals likely have been stabilized, physically and chemically, well above their Curie temperatures before or during final cooling. The NRM is a pure TRM and/or TCRM that appears to reside mainly in small PSD grains. Furthermore, for most samples inspected, no or hardly any chemical changes occur during laboratory heating up to ∼750°C, even when highly reduced magnetic minerals (αFe) are involved.

On the other hand, the exclusive normal-polarity remanence in all samples analyzed, might be alarming in view of the time they probably represent based on stratigraphic dating of overlying river deposits (from late Pliocene and early Pleistocene to recent; Table 1). The possibility that the NRM of burnt rocks represents a secondary VRM or even CRM due to weathering may not be excluded. After removal of a small viscous component, the NRM of all samples, however,

display univectorial decay to the origin. Moreover, other authors (Jones et al., 1984; Krsová et al., 1989; Tyráček, 1994) found reversed directions for several burnt rocks of Quaternary age. Virtually all thermal demagnetization diagrams by Jones et al. (1984) and Krsová et al. (1989) showed univectorial decay to the origin, similar to our AF demagnetization results.

Like lavas, the time period over which cooling, and thus remanence blocking, takes place, is a few years at most, and thus burnt rocks record a 'snapshot' of the ancient geomagnetic field. Furthermore, a particular burnt rock deposit formed over a few 100 years may contain a more or less continuous geomagnetic field record for that time interval. Individual burning events may occur intermittently, because the exposure of new coal seams is controlled by erosion or valley incision (cf. Tyráček, 1994; Zhang, 1999). This again may yield a record of directional and intensity change of the geomagnetic field. Studies by Jones et al. (1984) and Krsová et al. (1989) yielded promising results, but age determination of the burnt rocks appears to be a limiting factor of the use of burnt rocks for paleointensity and paleosecular variation determinations. Dating by fission-track, thermoluminescence and/or by means of stratigraphic correlation is possible but is of low precision. In addition, additional field evidence is necessary to exclude the possibility that reorientation of the sampled rock, for instance by overburden collapse, took place after TRM acquisition.

4.3.2. Magnetic anomaly modeling

The high NRM intensities and susceptibilities of the burnt rocks of the Xinjiang region are similar to data obtained on comparable rocks from other localities (e.g. Lindqvist et al., 1985; Krsová et al., 1989; Rădan and Rădan, 1998). For combustion-metamorphic rocks, the two parameters are typically between 0.1−10 A/m and 100×10^{-4} to 1000×10^{-4} SI, respectively. The αFe-bearing Gangou-samples fall outside these ranges and are anomalously low. Burnt rocks thus possess NRM intensities and χ_{lf} values that in general are two to three orders of magnitude higher than values typical of their sedimentary protoliths. As a consequence, the magnetic contrast between burnt rocks and the surrounding unaffected sedimentary rocks will likely produce magnetic anomalies. Indeed, Watson (1979), Lindqvist et al. (1985) and Rădan and Rădan (1998) observed strong magnetic anomalies between 500 and 2000 nT over exposed and unexposed burnt rock deposits by surface magnetic measurements, whereas Parker Gay and Hawley (1991) showed that anomalies associated with burnt rocks were sufficient to be recognized by aeromagnetic survey.

Magnetic properties of burnt rocks have potential for coal exploration and they can be used to delineate the areal extent and depth of (extinct) coal fires. In China, the spontaneous combustion of coal not only results in a substantial economic loss — estimated annual loss ∼10−20 million tonnes (Guan et al., 1996) — but also results in adverse environmental impacts by the release of smoke and noxious gases such as CO_x, NO_x, SO_2 and H_2S. Finally, combining magnetic anomaly data with remote sensing and field data can refine estimates of the actual and paleo-release of CO_2 by spontaneous combustion of coal in China.

5. Conclusions

Thermally altered sediments associated with burnt coal seams are high-fidelity geomagnetic field recorders, especially those in close vicinity to the remaining ash layer. They are suitable for paleointensity and paleosecular variation studies, although accurate age determinations are a limiting factor. The high NRMs and susceptibility values of these magnetically enhanced rocks approach those of extrusive igneous rocks and generally range of 0.1−10 A/m and 100×10^{-4} to 1000×10^{-4} SI, respectively. The principal remanence carriers in combustion-metamorphic rocks are relatively pure magnetite particles. In addition, relatively pure forms of maghemite, hematite and native iron, as well as complex spinel phases, can be present. The majority of the magnetic phases show rock-magnetic properties characteristic of small PSD particles. Native iron is likely present as SD more or less elongated particles capable of carrying a hard remanence. All magnetic phases show a high chemical and physical stability during heating in air. We infer that they are present as exsolution phases encased in host minerals. The extremes in oxidation degree of the iron phases indicate that conditions during combustion can vary between highly oxidizing to effectively reducing.

Acknowledgements

We gratefully acknowledge Dr. Xiangmin Zhang and Prof. Dr. Salle Kroonenberg for providing the combustion-metamorphic rocks. Piet-Jan Verplak measured some of the thermomagnetic runs. Tom Mullender upgraded the JR3 spinner magnetometer. This work was conducted under the programme of the Vening Meinesz Research School of Geodynamics (VMSG).

References

Argyle, K.S., Dunlop, D.J., 1990. Low-temperature and high-temperature hysteresis of small multidomain magnetites (215–540 nm). J. Geophys. Res. 95, 7069–7083.

Argyle, K.S., Dunlop, D.J., Xu, S., 1994. Single-domain behavior of multidomain magnetite grains. Eos (Trans. Am. Geophys. Un.), 75, Fall Meeting Suppl., 196 (Abstract).

Bentor, Y.K., Kastner, M., Perlman, I., Yellin, Y., 1981. Combustion metamorphism of bituminous sediments and the formation of melts of granitic and sedimentary composition. Geoch. Cosmoch. Acta 45, 2229–2255.

Bozorth, R.M., 1961. Ferromagnetism. Van Nostrand, New York, p. 968.

Cisowski, S., 1981. Interacting vs. non-interacting single domain behavior in natural and synthetic samples. Phys. Earth. Planet. Int. 26, 56–62.

Cosca, M.A., Essene, E.J., Geissman, J.W., Simmons, W.B., Coates, D.A., 1989. Pyrometamorphic rocks associated with naturally burned coal beds, Powder river basin, Wyoming. Am. Mineral. 74, 85–100.

de Boer, C.B., Dekkers, M.J., 1996. Grain-size dependence of the rock-magnetic properties for a natural maghemite. Geophys. Res. Lett. 23, 2815–2818.

de Boer, C.B., 1999. Rock-magnetic studies on hematite, maghemite and combustion-metamorphic rocks. Ph.D. Thesis, Utrecht University, Utrecht, The Netherlands, p. 256.

Deutsch, E.R., Rao, K.V., Laurent, R., Sequin, S.K., 1977. New evidence and possible origin of native iron in ophiolites of eastern Canada. Nature 269, 684–685.

Dunlop, D.J., Xu, S., 1993. A comparison of methods of granulometry and domain structure determination. Eos (Trans. Am. Geophys. Un.), 74, Fall Meeting Suppl., 203 (Abstract).

Dunlop, D.J., Özdemir, Ö., 1997. Rock Magnetism: Fundamentals and Frontiers. Cambridge University Press, Cambridge, p. 592.

Ellyett, C.D., Fleming, A.W., 1974. Thermal infrared imagery of the burning mountain coal fire. Remote Sens. Environ. 11, 221–229.

Foit Jr., F.F., Hooper, R.L., Rosenberg, P.E., 1987. An unusual pyroxene, melilite, and iron oxide mineral assemblage in a coal-fire buchite from Buffalo, Wyoming. Am. Mineral. 72, 137–147.

Gleason, J.D., Kyser, T.K., 1984. Stable isotope compositions of gases and vegetation near naturally burning coal. Nature 307, 254–257.

Guan, H.Y., 1984. The research of coal bed thermal IR radiation. In: Proceedings of the Seminars on Remote Sensing for Geological Applications, pp. 535–547.

Guan, H.Y., 1989. Applications of remote sensing techniques in coal geology. Acta Geol. Sin. 2, 254–269.

Guan, H.Y., Van Genderen, J.L., Schalke, H.J.W.G., 1996. Study and survey on the geological hazards of coal fire in North China. In: Proceedings of the 30th International Geological Congress Abstracts, Vol. 1, Beijing, China, p. 458.

Haggerty, S.E., Toft, P.B., 1985. Native iron in the continental lower crust: petrological and geophysical implications. Science 229, 647–649.

Harrison, R.J., Putnis, A., 1999. Determination of the mechanism of cation ordering in magnesioferrite ($MgFe_2O_4$) from the time- and temperature-dependence of magnetic susceptibility. Phys. Chem. Minerals 26, 322–332.

Jackson, M., 1991. Anisotropy of magnetic remanence: a brief review of mineralogical sources, physical origins, geological applications and comparison with susceptibility anisotropy. Pure Appl. Geophys. 136, 1–28.

Jones, A.H., Geissman, J.W., Coates, D.A., 1984. Clinker deposists, Powder river basin, Wyoming and Montana: a new source of high-fidelity paleomagnetic data for the Quarternary. Geophys. Res. Lett. 11, 1231–1234.

Kang, G.F., Zhang, Q.S., Lei, X.W., 1993. Coal fire investigation report of northern part of China (Northwest Area), ARSC Internal Report, Xian, China, 93 pp. (in Chinese).

Kneller, E., Luborsky, F.E., 1963. Particle size dependence of coercivity and remanence of single-domain particles. J. Appl. Phys. 34, 656–658.

Krsová, M., Krs, M., Pruner, P., Chvojka, R., 1989. Palaeointensity of the geomagnetic field during Upper Cainozoic derived from plaeo-slags and porcellanites in North Bohemia. Stud. Geophys. Geod. 33, 338–361.

Lindqvist, J.K., Hatherton, T., Mumme, T.C., 1985. Magnetic anomalies resulting from baked sediments over burnt coal seams in southern New Zealand. N.Z. J. Geol. Geophys. 28, 405–412.

Lowrie, W., Fuller, M., 1971. On the alternating field demagnetization characteristics of multidomain thermoremanent magnetization in magnetite. J. Geophys. Res. 76, 6339–6349.

Lowrie, W., 1990. Identification of ferromagnetic minerals in a rock by coercivity and unblocking temperature properties. Geophys. Res. Lett. 17, 159–162.

Mullender, T.A.T., Van Velzen, A.J., Dekkers, M.J., 1993. Continuous drift correction and separate identification of ferrimagnetic and paramagnetic contributions in thermomagnetic runs. Geophys. J. Int. 114, 663–672.

Parker Gay Jr., S., Hawley, B.W., 1991. Syngenetic magnetic anomaly sources: Three examples. Geophysics 56, 902–913.

Prakash, A., Gupta, R.P., Saraf, A.K., 1997. A Landsat TM based comparative study of surface and subsurface fires in the Jharia coalfield, India. Int. J. Remote Sens. 18, 2463–2469.

Rădan, S.C., Rădan, M., Rădan, S., 1994. Magnetic properties of sediments associated with coal seams: applications and implications. New Trends in Geomagnetism, Trešt, Czech Republic (Abstract).

Rădan, S.C., Rădan, M., 1998. Rock magnetism and paleomagnetism of porcelanites/clinkers from the western Dacic Basin (Romania). Geol. Carpat. 49, 209–211.

Roberts, A.P., Cui, Y., Verosub, K.L., 1995. Wasp-waisted hysteresis loops: mineral magnetic characteristics and discrimination of components in mixed magnetic systems. J. Geophys. Res. 100, 17,909–17,924.

Schneider, W., 1996. The coal-bearing Jurassic at the southern margin of the Junggar basin, Xinjiang. Geowissenschaften 14, 285–287.

Tauxe, L., Mullender, T.A.T., Pick, T., 1996. Potbellies, wasp-waists and super paramagnetism in magnetic hysteresis. J. Geophys. Res. 101, 571–583.

Tyráček, J., 1994. Stratigraphical interpretation of the paleomagnetic measurements of the porcellanites of the Most basin, Czech Republic. Vestnik Ceského geologického ústavu 69 (2), 83–87.

Ulff-Møller, F., 1990. Formation of native iron in sediment-contaminated magma. Part I. A case study of the Hanekammen Complex on Disko Island, West-Greenland. Geochim. Cosmochim. Acta 54, 57–70.

Van Genderen, J.L., Cassells, C.J.S., Zhang, X.M., 1996. The synergistic use of remotely sensed data for the detection of underground coal fires. International Archives of Photogrammetry and Remote Sensing, Vol. 31, No. B7. Vienna, pp. 722–727.

Verma, R.K., Prasad, S.N., 1975. Probable existance of native iron in newer dolerites from Singhbhum, Bihar, India. J. Geophys. Res. 80, 3755–3756.

Watson, D.E., 1979. Magnetic properties of clinkers (Abstract). Geophysics 44, 376–377.

Wilson, R.L., 1961. Paleomagnetism in Northern Ireland. Part I. The thermal demagnetization of natural magnetic moments in rocks. Geophys. J. R. Astr. Soc. 5, 45–58.

Zhang, X., 1998. Coal Fires in Northwest China: Detection, monitoring, and prediction using remote sensing data. Ph.D. Thesis, Delft University of Technology, Delft, The Netherlands, p. 135.